 doi:10.20944/preprints202101.0091.v1

Article

The Hydromechanical Interplay in the Three-dimensional Limit Equilibrium Analyses of Unsaturated Slope Stability

Panagiotis Sitarenios [1,*] and Francesca Casini [2]

[1] Coventry University, Coventry (UK); panagiotis.sitarenios@coventry.ac.uk (P.S.)
[2] Università degli Studi di Roma "Tor Vergata", Roma (IT); francesca.casini@uniroma2.it (F.C.)
* Correspondence: panagiotis.sitarenios@coventry.ac.uk;

Abstract: The paper presents a three-dimensional slope stability limit equilibrium solution for translational, planar failure modes. The proposed solution uses Bishop's average skeleton stress combined with the Mohr – Coulomb failure criterion to describe soil strength evolution under unsaturated conditions while its formulation ensures a natural and smooth transition from the unsaturated to the saturated regime and vice versa. The proposed analytical solution is evaluated by comparing its predictions with the results of the Ruedlingen slope failure experiment [1]. The comparison suggests that despite its relative simplicity the analytical solution can capture well the experimentally observed behaviour and highlights the importance of lateral resistance consideration together with a realistic interplay between mechanical parameters (cohesion) and hydraulic (pore water pressure) conditions.

Keywords: unsaturated slope; Ruedlingen field experiment; lateral resistance; limit equilibrium solution

1. Introduction

It is well known that partial saturation can play a key role in stabilizing both natural and artificial slopes. The interparticle forces due to the forming water menisci at the macrostructure and/or intermolecular forces due to absorptive and osmotic phenomena increase the shear strength of geomaterials improving stability conditions. Loss of this beneficial contribution can significantly hinder stability conditions and trigger slope failures. A characteristic example is rainfall induced landslides which comprise one of the most common geotechnical failures [2–4].

Rainfall induced landslides is one example of the significance that unsaturated soil mechanics can have in engineering problems, with other characteristic representatives being expansive and collapsible soils. Unfortunately, despite its significant importance in many geotechnical problems, unsaturated soil mechanics still struggles today to find its room in everyday geotechnical practice. The reasons are usually related to the relative complexity of the material laws involved (i.e., water retention behaviour), the increased complexity of the required laboratory tests (i.e., suction controlled shear strength determination) and on the lack of simple calculation tools accessible to everyday practitioners with fundamental knowledge of soil mechanics.

In that respect, the present paper presents and evaluates a simple slope stability limit equilibrium solution for translational failure modes. The proposed solution is initially derived under two-dimensions (2D) and it is later extended to three dimensions (3D) by additionally examining the potential development of shear strength along the sides of a sliding block with finite lateral dimension. Similar solutions for unsaturated soil conditions exist in the international literature [1,5–7] however, usually they involve assumptions which prevent them from remaining valid under saturated conditions especially when positive pore water pressures appear. The most common reasons are either

 doi:10.20944/preprints202101.0091.v1

the use of stress parameters which cannot recall Terzaghi's effective stress upon saturation or assumptions with respect to the lateral in-situ stress and its evolution with partial saturation which are incompatible with classical soil mechanics principles.

The proposed stability solution is derived as a natural extension of classical soil mechanics which is key in facilitating the adoption of such solutions in engineering practice [4]. To evaluate the proposed solution, this is applied to the analyses of a well instrumented field experiment where a slope failure was triggered by means of artificial rainfall, the Ruedlingen experiment [1,8]. It proves that despite its simplicity the proposed mechanism can represent very satisfactorily the experimentally observed behaviour both qualitatively and quantitatively. The presented discussion highlights the importance of considering the lateral development of the failure mechanism (3D) and of the natural transition to the saturated domain in capturing the behaviour.

2. A Slope Stability Limit Equilibrium Solution for Translational Modes in Unsaturated Soils.

This section discusses the limit equilibrium stability calculation of a simple translational slope stability mechanism. Firstly, the assumed geometry is introduced and simple actions such as the weight of the sliding block are calculated. Then the shear resistance along the failure plane is calculated considering the effect that partial saturation has on soil shear strength. Finally, the Factor of Safety (FoS) against failure is formulated by additionally considering the lateral resistance developing at the sides of a 3D failing soil block.

3.1. The assumed Failure Mechanism

Figure 1 shows the assumed failure mechanism. A soil layer of thickness z rests on top of another material, the latter assumed a priory of infinite strength. Both the soil surface and the interface between the two materials is described by two parallel planes with an inclination θ with the horizontal. The interface between the two materials acts as a potential failure surface (plane) and a simple translational failure mechanism develops where the upper layer tends to slide along the interface.

To examine such a typical translational failure mechanism, we can isolate a block of soil with length of l=1m along the x-axis which is the one parallel to the failure plane as shown in Figure 1. To obtain an initial solution for a two-dimensional (2D) failure mechanism an analyses per running meter is performed. The soil is assumed homogeneous and isotropic while suction (s) and degree of saturation (S_r) are both assumed constant along the entire soil layer with no variation with depth in favour of simplicity. Moreover, for the sake of generality of the produced solution a vertical surcharge equal to q is assumed on the surface of the soil.

Preprints (www.preprints.org) | NOT PEER-REVIEWED | Posted: 5 January 2021 doi:10.20944/preprints202101.0091.v1

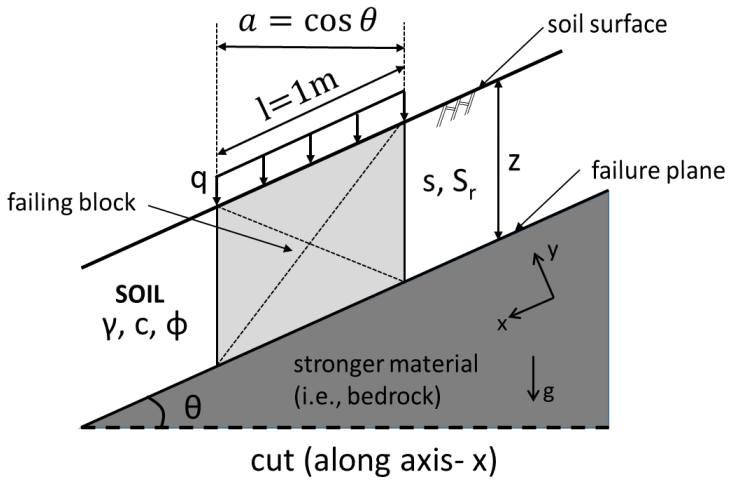

Figure 1. The analyzed translational failure mechanism along a planar failure surface with slope θ.

The unit weight of the soil varies with degree of saturation (S_r) following Equation 1 as:

$$\gamma = \frac{G_S + e \cdot S_r}{1 + e} \cdot \gamma_w \,, \quad (1) \quad (1)$$

where G_s the specific gravity and e the void ratio of the soil while γ_w the unit weigh of the water usually assumed equal to $\gamma_w = 9.81kN/m^3$. Having defined the unit weight of the soil, the weight of the soil block (W) can be calculated and analyzed to two components W_x and W_y, along the x and y axis respectively, as shown in Figure 2a:

$$W = \gamma \cdot z \cdot \cos\theta, \quad (2a)$$

$$W_x = W \cdot \sin\theta = \gamma \cdot z \cdot \cos\theta \cdot \sin\theta, \quad (2b)$$

$$W_y = W \cdot \cos\theta = \gamma \cdot z \cdot \cos^2\theta, \quad (2c)$$

To further consider the effect of the uniform surcharge we calculate the corresponding force (Q) and its two components Q_x and Q_y, along the x and y axis respectively, as shown in Figure 2a:

$$Q = q \cdot \cos\theta, \quad (3a)$$

$$Q_x = Q \cdot \sin\theta = q \cdot \cos\theta \cdot \sin\theta, \quad (3b)$$

$$Q_y = Q \cdot \cos\theta = q \cdot \cos^2\theta. \quad (3c)$$

Finally, as portrayed in Figure 2b, the sum of the forces due to: a) the weight of the soil block and b) the surcharge is considered; initially on the x-axis where F_x plays the role of the destabilizing action trying to slide the considered block along the failure surface,

$$F_x = Q_x + W_x = q \cdot \cos\theta \cdot \sin\theta + \gamma \cdot z \cdot \cos\theta \cdot \sin\theta = (q + \gamma z)\ \cos\theta \cdot \sin\theta, \quad (4)$$

and, along the y- axis where F_y is equal to the reaction force from the bottom layer:

Preprints (www.preprints.org) | NOT PEER-REVIEWED | Posted: 5 January 2021 doi:10.20944/preprints202101.0091.v1

$$N = F_y = Q_y + W_y = q \cdot cos^2\theta + \gamma \cdot z \cdot cos^2\theta = (q + \gamma z)\ cos^2\theta. \quad (5)$$

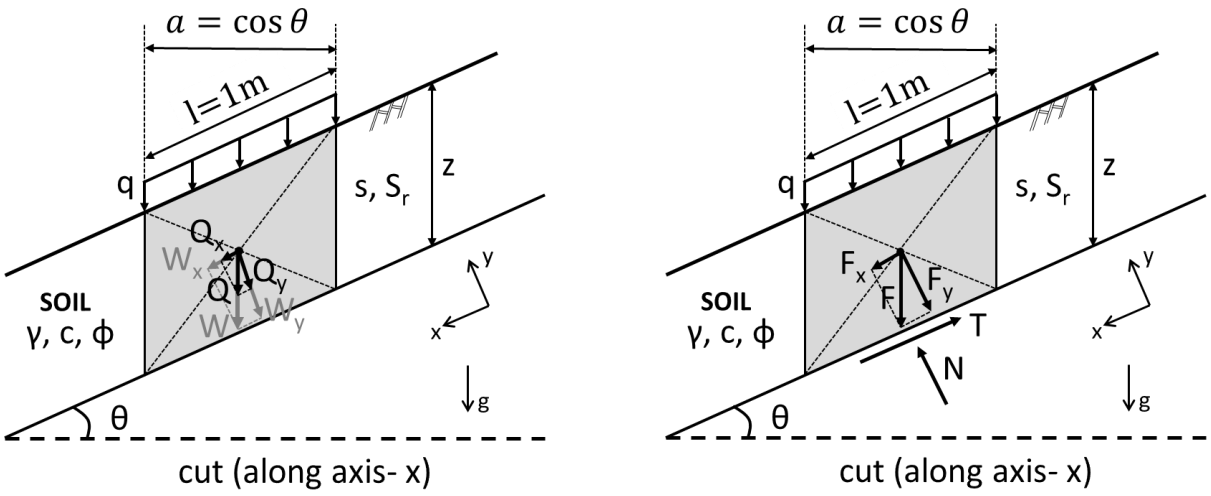

(**a**) (**b**)

Figure 2. (**a**) Analyses of the weight of the block and of the applied surcharge; (**b**) The equilibrium of the block along x-axis (parallel to the failure plane) and y-axis (perpendicular to the failure plane).

3.2. Shear Resistance Under Unsaturated Conditions

The shear resistance at the interface is assumed to be entirely controlled by the shear strength parameters of the soil block and is described by the Mohr – Coulomb failure envelope. The effect of partial saturation on shear strength is considered by using Bishop's (average) skeleton stress [9]. Bishop's average skeleton stress (σ') is calculated according to Equation 6 as the sum of the total stress (σ) plus suction ($s = -u_w$, assumed air pressure: $u_a = 0$), the latter scaled for a parameter χ.

$$\sigma' = \sigma + s \cdot \chi, \quad (6)$$

It is clarified that although the prime symbol is used for Bishop's average skeleton stress, this should not be considered an effective stress variable; in fact, a second stress variable must be defined to adequately describe the behaviour of unsaturated soils, e.g. suction s. If χ is properly selected to correspond to $\chi = 1$ upon full saturation ($S_r = 1.0$) and to $\chi = 0$ for dry states ($S_r = 0.0$) then Bishop's skeleton stress recalls Terzaghi's effective stress upon saturation which is a desirable feature for the unified description of saturated and unsaturated material states.

The Bishop's skeleton stress combined with common failure criteria for soils proves adequate when the interest focuses exclusively on the evolution of shear strength with partial saturation. This is supported by an ensemble of different studies [10–13] all of them suggesting that χ must be a function of S_r which ensures $\chi = 1$ for $S_r = 1.0$ and to $\chi = 0$ for $S_r = 0.0$, as previously discussed.

In that end, for the examined sliding block failure mechanism the shear resistance along the interface is described by the Mohr - Coulomb failure criterion combined with Bishop's skeleton stress:

$$\tau = c + \{\sigma + s \cdot \chi\} \cdot tan\,\phi \quad (7)$$

where τ the shear strength of the material described by the well-known shear strength parameters cohesion (c) and angle of internal friction (ϕ). The failure criterion is now

Preprints (www.preprints.org) | NOT PEER-REVIEWED | Posted: 5 January 2021 doi:10.20944/preprints202101.0091.v1

applied at the failure surface of the examined stability mechanism to calculate that the shear resistance force (T) (see also Figure 2b) can be calculated as (see also Appendix A):

$$T = c + (q + \gamma z)\ cos^2\theta \cdot tan\phi + s \cdot \chi \cdot tan\phi \quad (8)$$

Figure 2. D failure mechanism the Factor of Safety (FoS) can be calculated according to:

$$FoS = \frac{T}{F_x} = \frac{\frac{c}{cos^2\theta} + \frac{s \cdot \chi \cdot tan\phi}{cos^2\theta} + (q + \gamma z)\ tan\phi}{(q + \gamma z)\ tan\theta} \quad (9)$$

3.2. Extension to 3D – Lateral Shear Resistance

The simple 2D translational slope failure mechanism presented hereinbefore and quantified through Equation 7 can be used to evaluate the stability of planar slope instabilities where failure extends enough to reasonably assume that stability can be evaluated by performing a "per running meter analyses" where a slice of the falling mass with thickness of 1m at the center of the failure area is isolated and studied. However, in many cases, slope failures have rather finite dimensions where the aforementioned assumption gets problematic.

In such cases the main shortcoming of the 2D mechanism is that it neglects the contribution of the shear resistance developing at the sides of the failing mass. Neglecting their contribution proves conservative and usually this is the justification accompanying the assumption of simple 2D slope stability methods in the design of slopes and cuts. However, this is not true when it comes to the back analyses of slope failures where neglecting the actual dimensions of the failure mass and the contribution of the lateral resistance can significantly hinder the outcome of the analyses (i.e., overestimation of soil shear strength parameters and/or suction contribution).

In that end, this section extends the discussed translational failure mechanism in the 3D domain by additionally considering the contribution of lateral resistance. In doing so, the geometry of Figure 3 is considered. The failing block has now a width (b) which limits its lateral development, while similar to the 2D mechanism, the depth of the failure mass is (z) and the length is $l = 1m$ which as horizontal distance translates to $a = \cos\theta$.

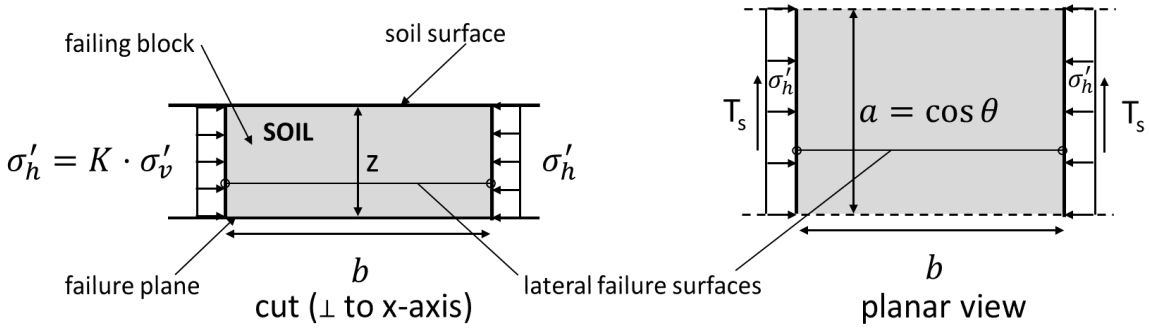

Figure 3. The 3D failure mechanism in cut and planar view.

To calculate the shear resistance T_s developing along each of the two lateral sides of the block, the Mohr - Coulomb failure criterion combined with Bishop's average skeleton stress will be used again. The horizontal stress at the two lateral interfaces is assumed to be equal to $\sigma'_h = K \cdot \sigma'_v$ where K a coefficient of lateral earth pressure. Applying the lateral earth pressure coefficient to Bishops' stress as opposed to total stress that other solution assume (i.e., [1]) makes the derived solution applicable under positive pore water pressure regimes as well, while recent experimental evidence on soil anisotropy and

Preprints (www.preprints.org) | NOT PEER-REVIEWED | Posted: 5 January 2021 doi:10.20944/preprints202101.0091.v1

partial saturation [14] also support such an assumption. The vertical Bishop's skeleton stress is calculated in the middle of the depth (z) as:

$$\sigma_v' = \sigma_v + s \cdot \chi = q + \gamma \cdot \frac{z}{2} + s \cdot \chi \tag{10}$$

and the corresponding horizontal stress as:

$$\sigma_h' = K \cdot \sigma_v' = K \cdot q + K \cdot \gamma \cdot \frac{z}{2} + K \cdot s \cdot \chi \tag{11}$$

Table 12. here c_s and ϕ_s the cohesion and frictional resistance respectively along the lateral sides of the failure block. They are assumed different from their soil counterparts in favour of generality of the solution, by allowing different shear strength parameters to be assigned to the lateral resistance. Having defined the shear strength along the two lateral sides we can then also calculate the corresponding shear resistance, where after some algebra (see Appendix B) the following expression is derived:.

$$T_s = c_s \cdot z \cdot \cos\theta + K \cdot q \cdot z \cdot \cos\theta \cdot \tan\phi_s + K \cdot \gamma \cdot \frac{z^2}{2} \cdot \cos\theta \cdot \tan\phi_s + K \cdot s \cdot \chi \cdot z \cdot \cos\theta \cdot \tan\phi_s \tag{13}$$

Finally using the additional resistance along the sides of the 3D mechanism, the safety factor against sliding is reformulated:

$$FoS = \frac{T + \frac{2T_s}{b}}{F_x} \tag{14}$$

Note that the additional resistance at the two sides ($2T_s$) is normalized over the width (b) of the block to combine it mathematically with the already determined resistance T and action F_x for the 2D mechanism. Finally, by using equations 4, 8 and 13 to substitute for F_x, T and T_s respectively in Equation 14 we can calculate that the Factor of Safety (FoS) against sliding for the 3D mechanism as:

$$FoS = \frac{\frac{c}{\cos^2\theta}\left(1 + \frac{2\rho_c \cos\theta}{b}\right) + \frac{s\chi\tan\phi}{\cos^2\theta}\left(1 + \frac{2\rho_\phi Kz\cos\theta}{b}\right) + q \cdot \tan\phi\left(1 + \frac{2\rho_\phi Kz}{b \cdot \cos\theta}\right) + \gamma z \cdot \tan\phi\left(1 + \frac{\rho_\phi Kz}{b \cdot \cos\theta}\right)}{(q + \gamma z) \cdot \tan\theta} \tag{15}$$

In Equation 15 and in order to obtain a more elegant solution the shear strength parameters used for the resistance along the inclined failure surface and along the sides of the block have been correlated using the following factors:

$$\rho_s = \frac{c_s}{c} \tag{16a}$$

$$\rho_\varphi = \frac{\tan\phi_s}{\tan\phi} \tag{16b}$$

3. Evaluation Using an Actual Case

To evaluate the planar slope stability mechanism previously presented and to demonstrate the potential importance of lateral resistance in analysing slope instabilities the results from the Ruedlingen full scale experiment [1,15] will be used and compared with the predictions of the proposed stability mechanism.

3.1. The Ruedlingen Full Scale Experiment

The Ruedlingen full scale field test [1,15] was performed to study the response of a steep forested slope, subjected to artificial intense rainfall within the context of the multi-disciplinary research programme on "Triggering of Rapid Mass Movements in steep terrain" (TRAMM). The experiment was carried out in northern Switzerland in a forested

Preprints (www.preprints.org) | NOT PEER-REVIEWED | Posted: 5 January 2021 doi:10.20944/preprints202101.0091.v1

area near Ruedlingen village. The selected experimental site was located on the east-facing bank of the river Rhine, with an average slope angle of approximately 38°. An orthogonal area, with a length of 35m and a width of 7.5m, was instrumented with a wide range of devices (see Figure 3b). A landslide triggering experiment was conducted in March 2009 where the slope was subjected to artificial rainfall with an average intensity of 20mm/h at the upper approximately one third of the slope and with 7mm/h in the remaining lower part leading to a shallow slope failure after 15 hours.

The failure concentrated at the upper part of the instrumented area (see Figure 3b) and extended within a surficial layer of a medium to low plasticity (average PI~10%) silty sand (ML) [16]. This soil layer rests on top of a fissured Molassic bedrock (sandstone and marlstone - see Figure 3a) [17,18]. Sitarenios *et al.* [8] analysed numerically the triggered slope instability and combining field measurements with numerical results they concluded that failure happens under saturated conditions and it is triggered by water exfiltration from the bedrock which results to considerable pore water pressure build up at the soil – bedrock interface.

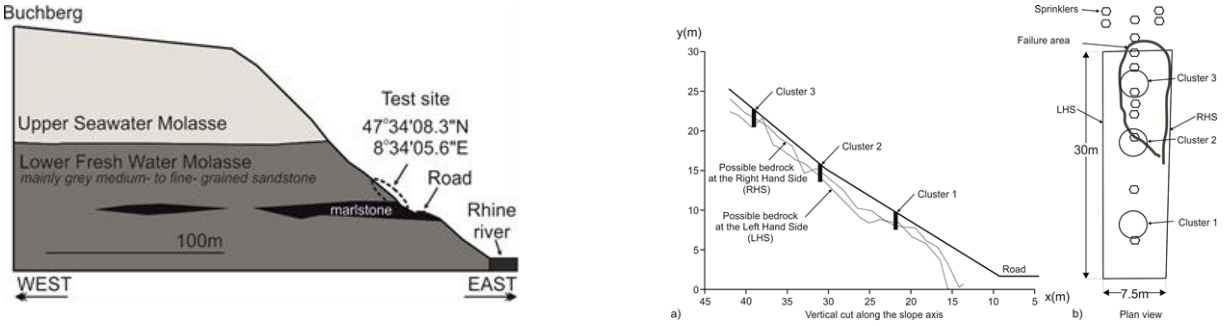

Figure 3. (**a**) Geomorphology of the greater experimental area (after [17]); (**b**) a schematic of the bedrock topography and of the instrumented area of the experiment (after [19]).

3.2. 2D Solution – Neglecting Lateral Resistance

In this section the proposed limit equilibrium mechanism is used to evaluate the stability of the Ruedlingen slope by neglecting any contribution of lateral resistance or in other words by assuming an infinite failure mechanism perpendicular to the examined plane. In utilizing the mechanism it is important to first establish the hydraulic and mechanical parameters of the Ruedlingen soil, while to enable comparison of the results with the study of Sitarenios *et al.* [8] the same experimental data will be examined and similar assumptions will be put forward.

Starting with the hydraulic behaviour, as discussed with Equation 7, calculation of the shear strength of the soil under unsaturated conditions necessitates knowledge of the degree of saturation as the latter is the most commonly made assumption for parameter (χ). To calculate degree of saturation and thus parameter (χ) the Water Retention Model (WRM) of equation (15a) is used where s is the suction level, b_w is a model parameter controlling the shape of the reproduced Water Retention Curve (WRC) and $S_{r,max}$ & $S_{r,min}$ are the maximum and residual degree of saturation, respectively. It is a Van Genuchten WRM [20] which includes dependence of the behaviour of the void ratio ($e = n/(1-n)$) through parameter P as described in equation (15b), where P_0 and n_0 are reference values and parameter a_w controls the rate of change of the WRC with void ratio.

$$\chi = S_r = S_{r,res} + \left(S_{r,max} - S_{r,res}\right)\left[1 + \left(\frac{s}{P}\right)^{\frac{1}{1-b_w}}\right]^{-b_w} \quad (15a)$$

Preprints (www.preprints.org) | NOT PEER-REVIEWED | Posted: 5 January 2021 doi:10.20944/preprints202101.0091.v1

$$P = P_0 \cdot \exp[\alpha_w(n_0 - n)] \quad (15b)$$

The water retention behaviour is calibrated based on a set of suction controlled wetting laboratory test [21] . The calibrated behaviour can be seen in Figure 4a and the parameters used in Table 1. Figure 4b shows the WRC curve that is used in the analyses and it is the one corresponding to an initial void ratio of $e = 0.9$ as this has been measured in the field and used in previous studies [8]. It is accompanied by the evolution of the $s \cdot S_r$ term which in fact reflects the increase in the shear strength of the material with suction.

Table 1. Ruedlingen WRM Parameters Used in this Study.

Parameter	Value	Parameter	Value
P_0 (kPa)	0.65	α	21.0
b_w	0.4	n_0	0.47
$S_{r,max}$	1.0	$S_{r,min}$	0.33

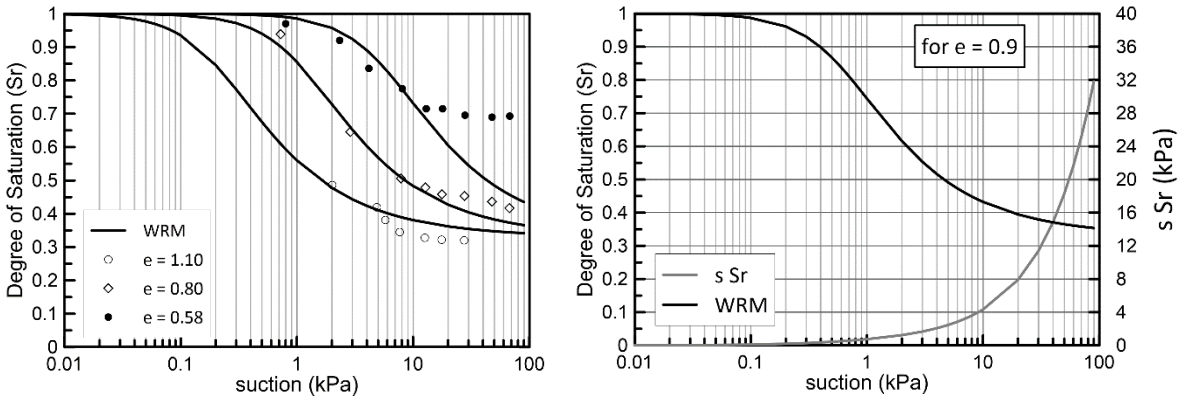

(**a**) (**b**)

Figure 4. (**a**) The calibrated WRM (laboratory data from [21]); (**b**) the WRC used in the analyses with the corresponding evolution of the $s \cdot S_r$ term.

With the WRM calibrated, Equation 7 is used to calculate the safety factor of the Ruedlingen slope under different combinations of suction and slope height. With respect to the shear strength parameters involved in Equation 7, cohesion is set zero ($c = 0$) and the friction angle equal to $\phi = 32^o$ [8,16], while the unit weight (γ) of the slope follows the evolution of saturation through Equation 1 with specific gravity taken equal to $G_s = 2.65$. Finally, the inclination of the failure surface is set equal to the average inclination of the slope ($\theta = 38^o$) [1] and no surcharge is considered on the soil surface ($q = 0$).

Figure 5 presents the results of a parametric study. Figure 5a portrays the evolution of the FoS with suction for various slope heights ranging from 0.5 to 2.75m. The reason why the height of the slope is handled parametrically is related to the in-situ variability of the thickness of the soil layer which was found to range from 0.5m to 4.5m [15,17] in general while in the part of the slope where failure occurred the variation was smaller with depths up to 2.75m. In figure 5b similar results are presented with depth in the horizontal axis and the various curves representing different suction levels from zero up to 10kPa, values within the range of the in situ initial suction values as those have been reported in [15].

The results of Figure 5 clearly demonstrate the dominant effect that partial saturation can have in stabilizing a planar slope stability mechanism. It is characteristic that

Preprints (www.preprints.org) | NOT PEER-REVIEWED | Posted: 5 January 2021 doi:10.20944/preprints202101.0091.v1

when no suction is present ($s = 0$), a cohesionless slope ($c = 0$) has a safety factor which is constant to the $\frac{tan(\phi)}{tan(\theta)}$ ratio which for the examined slope geometry and for the Ruedlingen soil shear strength is equal to $\frac{tan(32^o)}{tan(38^o)} = 0.8$. In both Figures 5a & 5b it is observed that even a small suction increase, significantly alters stability conditions with various combinations of suction and slope height exhibiting even a stable behaviour (FoS≥1).

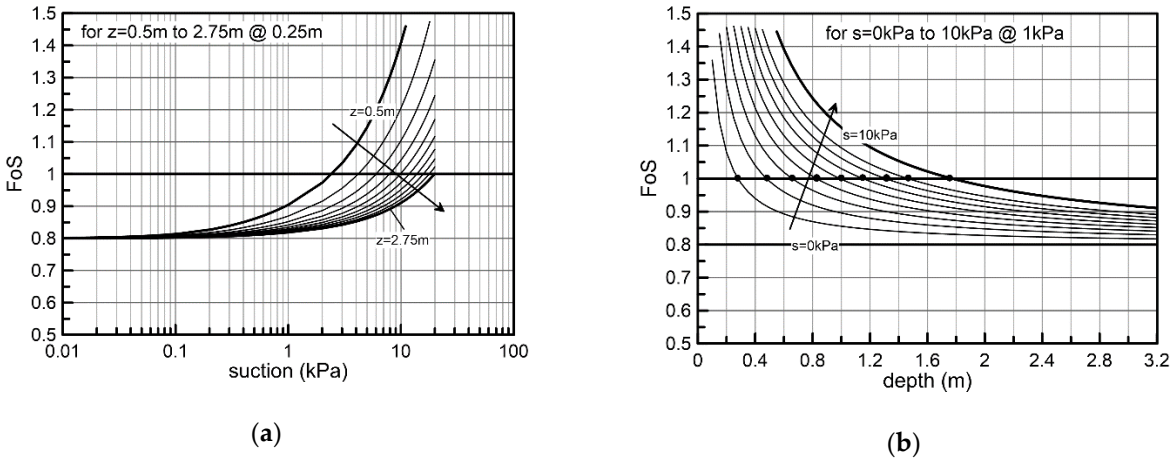

(**a**) (**b**)

Figure 5. (**a**) evolution of FoS with suction for different slope heights; (**b**) evolution of FoS with slope height for different suction levels; Results from a 2D mechanism (no lateral resistance).

To better understand this interplay between the height of the slope and suction, Figure 6 presents stability charts correlating the two quantities, with suction in the horizontal and slope height in the vertical axis, respectively. Figure 6a suggests that there is an almost linear relation between the increase in depth and the required increase in suction for the slope to remain stable (FoS>1), while in Figure 6b the same relation is presented using a logarithmic scale with suction. Figure 6b helps to understand that the increase in the stable slope height with suction in fact follows the trend of the increase in the shear strength with suction as the latter is controlled by the increase in the $s \cdot S_r$ term in Figure 4b.

Examining the stability chart of Figure 6 in relation to the observed behaviour during the Ruedlingen field experiment it seems that the suggested evolution of stability with suction and slope height does not match the observed behaviour. If we consider an average slope height of 1.5 to 2m, Figure 6 suggests that a minimum suction value of 10 to 15kPa is required for stability. This may partially explain why the slope remains stable under the initial hydraulic regime which suggests a value of around 10 kPa but at the same time it is obvious that even the smallest decrease in suction should cause failure. However, both in-situ measurements [1] and numerical analyses [8] clearly indicate that even complete loss of suction is not enough to trigger the Ruedlingen failure. In that respect it seems reasonable to assume that additional factors contribute to stability with respect to those examined with the present 2D failure mechanism.

Preprints (www.preprints.org) | NOT PEER-REVIEWED | Posted: 5 January 2021 doi:10.20944/preprints202101.0091.v1

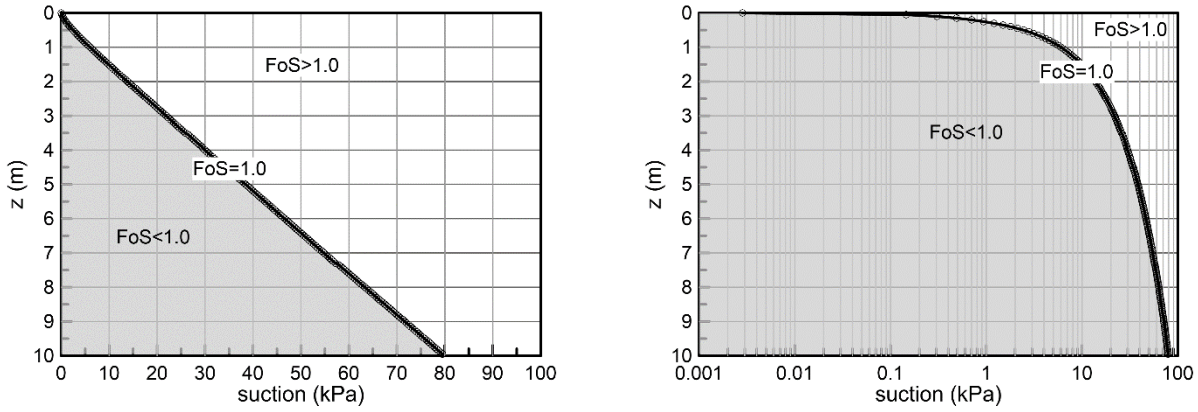

(**a**) (**b**)

Figure 6. Stability chart; (**a**) stable vs unstable suction and slope height combinations; (**b**) as (a) in a semilogarithmic plot; Results from a 2D mechanism (no lateral resistance).

3.3. 3D solution – Including Lateral Resistance

Lateral resistance can be one of the factors contributing to improved stability conditions with respect to those of Figure 6. To consider the effect of lateral resistance in the examined problem the analysis of the previous section is repeated by additionally considering that lateral resistance develops at the two sides of a failing block with a width equal to b=7.5m. For the side resistance the same friction angle as for the soil – bedrock interface is assumed (ρ_ϕ=1.0), while for the lateral earth pressure coefficient an arbitrary value of K=0.5 is chosen, close to the value suggested by Jaky's formula for $\phi = 32^o \Rightarrow K = 1 - \sin 32 = 0.47$.

Figure 7 presents results similar to those of Figure 5 however, in this instance, including the additional contribution of lateral resistance. The results clearly demonstrate the beneficial effect of lateral resistance in increasing FoS under given combinations of slope height and suction. It is interesting to observe that Figure 7a seems to suggest that the effect of suction in improving stability conditions becomes less profound as the slope height increases. Moreover, Figure 7b indicates that under relatively small slope height values (i.e., less than 0.6m) the influence of suction is quite significant while as the slope height increases its effect gest less profound, reaches a minimum for a given depth and then slightly increases again.

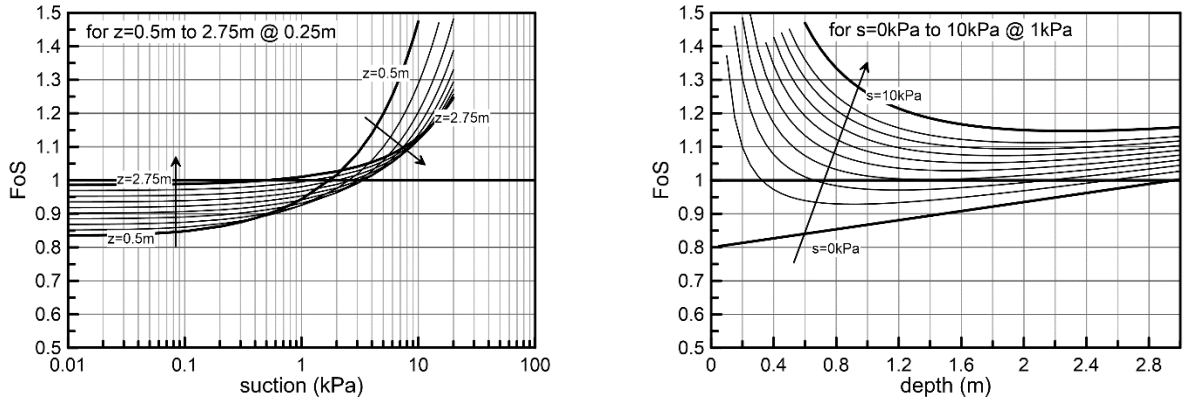

(**a**) (**b**)

Figure 7. (**a**) evolution of FoS with suction for different slope heights; (**b**) evolution of FoS with slope height for different suction levels; Results from a 3D mechanism (with lateral resistance).

Preprints (www.preprints.org) | NOT PEER-REVIEWED | Posted: 5 January 2021 doi:10.20944/preprints202101.0091.v1

This is better profound in Figure 8 which presents a stability chart similar to Figure 6 with the addition of the lateral resistance. It is observed that as the height of the slope increases, positive pore water pressure values are needed to cause instability. Qualitatively, this trend in behaviour is much better aligned with the behaviour of the Ruedlingen slope where failure happened following considerable water pressure built-up which reduced the available shear strength at the soil bedrock interface. Moreover, both post failure in situ observations and numerical results suggest that the depth of the failure surface ranged from 1.0 to 2.0m. This is in good agreement with Figure 8, where within the same range of z values the stability chart exhibits a peak coinciding with the most unfavourable stability conditions for the given assumptions.

However, from a quantitative perspective and withing the same range of slope height the required suction for stability suggests that the slope should have failed before reaching full saturation contrary to what was observed in situ. This discrepancy can be attributed to several factors which can result to better stability conditions than those described by the analysis used for this study. Amongst others, two of the most likely potential candidates for the different behaviour can be a) the presence of some cohesion either due to fines or due to the contribution of vegetation and roots [22]; b) a less extended mechanism in the third direction (smaller b) and; c) a different WRC. However, it should be recognized that the WRC can only affect the behaviour in the unsaturated regime and still cannot explain why a higher positive pore water pressure may be needed to trigger the instability.

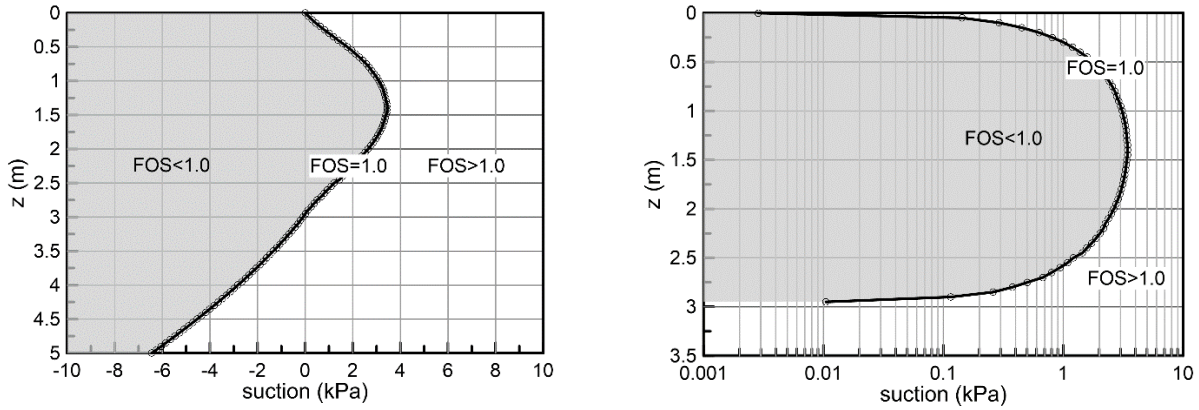

Figure 8. Stability chart; (**a**) stable vs unstable suction and slope height combinations; (**b**) as (a) in a semilogarithmic plot; Results from a 3D mechanism (with lateral resistance).

3.3. 3D solution – the Effect of Cohesion and 3D mechanism Development.

The previous section demonstrated how the inclusion of the lateral resistance in the analyses can justify an improvement of the stability conditions for the analyzed Ruedlingen field experiment. However, it was not feasible to quantitatively approach the behaviour satisfactorily. As mentioned in the previous section either the presence of cohesion or a narrower than the assumed mechanism can serve as the most probable explanations and this hypothesis is putted into test in the section.

To examine what is the effect of different assumptions regarding the aforementioned factors a parametric analysis is done to check the sensitivity of the stability charts on the presence of cohesion (c) and on the width (b) of the 3D mechanism. Figure 9(a) presents how the stability curve differentiating between stable and unstable conditions changes with an increase in cohesion. Five different cohesion values namely $c = 0, 1, 2, 3, 4$ and 5 kPa (from the blue to the red curve) are examined and the same cohesion values also apply to the lateral resistance by assuming $\rho_c = 1.0$ in Equation 16.

Preprints (www.preprints.org) | NOT PEER-REVIEWED | Posted: 5 January 2021 doi:10.20944/preprints202101.0091.v1

The plotted charts indicate a significant contribution of cohesion to stability conditions. Even the smallest nonzero value of $c = 1$ kPa is enough to justify a stable slope under the presence of the smallest suction and irrespective of its height. This is in accordance with the experimentally observed behaviour while the presence of roots can justify even higher values of cohesion [22] which if adopted (i.e., $c = 5$kPa) can alone explain why in the Ruedlingen experiment, significant pore pressures up to almost 10 kPa where needed in the soil bedrock interface for failure to occur.

Figure 9d offers a similar discussion by explaining the effect of the width of the assumed mechanism. The main assumption putted forward in the analyses presented hitherto is that the width of the mechanism is $b = 7.5$m coinciding with the width of the experimental area (dashed curve on Figure 9b). However, the in-situ post failure observations suggest that the failing mass had a smaller average width (see also Figure 3b) and simultaneously the results of Figure 9b indicate that such a reduction in the lateral development of the failure mechanism is quite beneficial for stability. In more detail, Figure 9b presents the evolution of the stability curves with the width of the mechanism, namely from $b = 7$m down to $b = 1$m (from the blue to the red curve). It is interesting to observe that the effect of lateral development is qualitatively different compared to that of cohesion, with the slope height playing a key role as well. Observe that as the slope becomes higher and the mechanism narrower the effect of the lateral resistance on improving stability becomes higher. This is a clear reflection of the fact that the ratio of the area of the lateral side over the area of the soil bedrock interface becomes higher, increasing the contribution of the side resistance and limiting the contribution of the failure plane resistance, thus making progressively the lateral resistance more and more dominant.

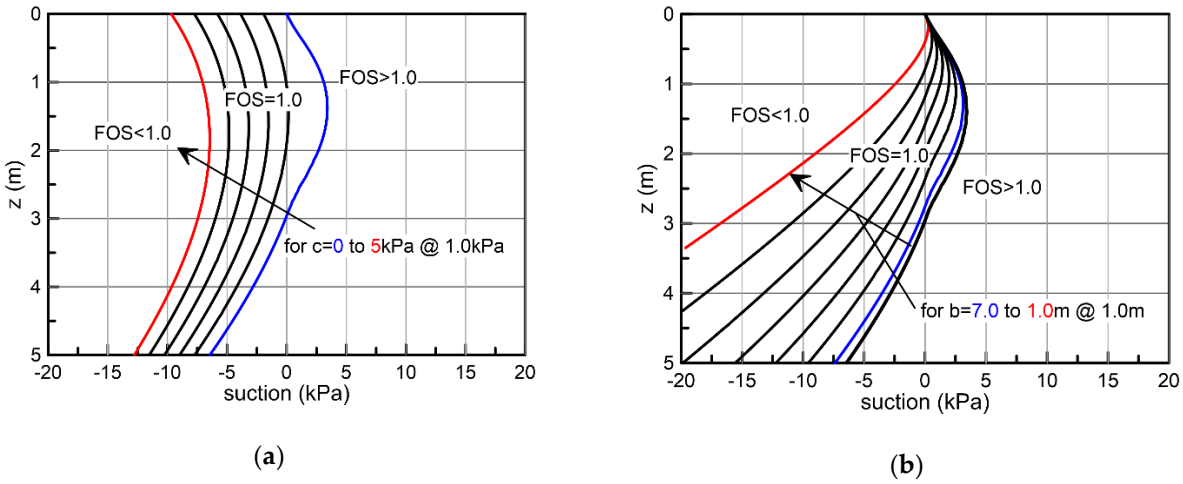

(**a**) (**b**)

Figure 9. (**a**) effect of cohesion on the stability chart; (**b**) effect of the 3D mechanism width on the stability chart; Results from a 3D mechanism (with lateral resistance).

Regarding the in-situ behaviour, it is clear that a narrower mechanism cannot alone explain the in situ behaviour, as for the slope height relevant to the Ruedlingen soil (z =1 to 2m) and the range of the lateral development of the mechanism (b =5 to 7m), the slope is still unstable, even though there is a noticeable improvement in stability conditions with respect to the refence scenario (b =7.5m). In that respect, the best candidate to justify the experimental behaviour is cohesion. From the results of Figure 9 it seems that reasonable assumptions regarding a small presence of cohesion in the order of c =3 to 4kPa, combined with a relatively smaller average mechanism b =5 to 7m can explain very satisfactory the experimentally observed behaviour during the Ruedlingen experiment both qualitatively and quantitively.

To test this assumption, four combinations of cohesion and slope width within the aforementioned range of values are analysed in Figure 10b. In the same graph, the grey

Preprints (www.preprints.org) | NOT PEER-REVIEWED | Posted: 5 January 2021 doi:10.20944/preprints202101.0091.v1

shaded area indicates the range of values of slope height and "suction" (negative suction values correspond to positive pore water pressure) most representative of the in-situ failure conditions. In more detail, Figure 10a presents the failure mechanism (after [1]) where the average depth of the failure surface was at more than 1m. It also contains a plot of the evolution of the in-situ and of the numerically determined pore water pressure at the failure area (after [8]) indicating that an average pore water pressure in the order of 5kPa was present in the slope mass at failure. The very good much of the stability curves with the shaded area is a clear indication that the relatively simple 3D translational failure mechanism used in this study can provide a very good insight into the Ruedlingen failure.

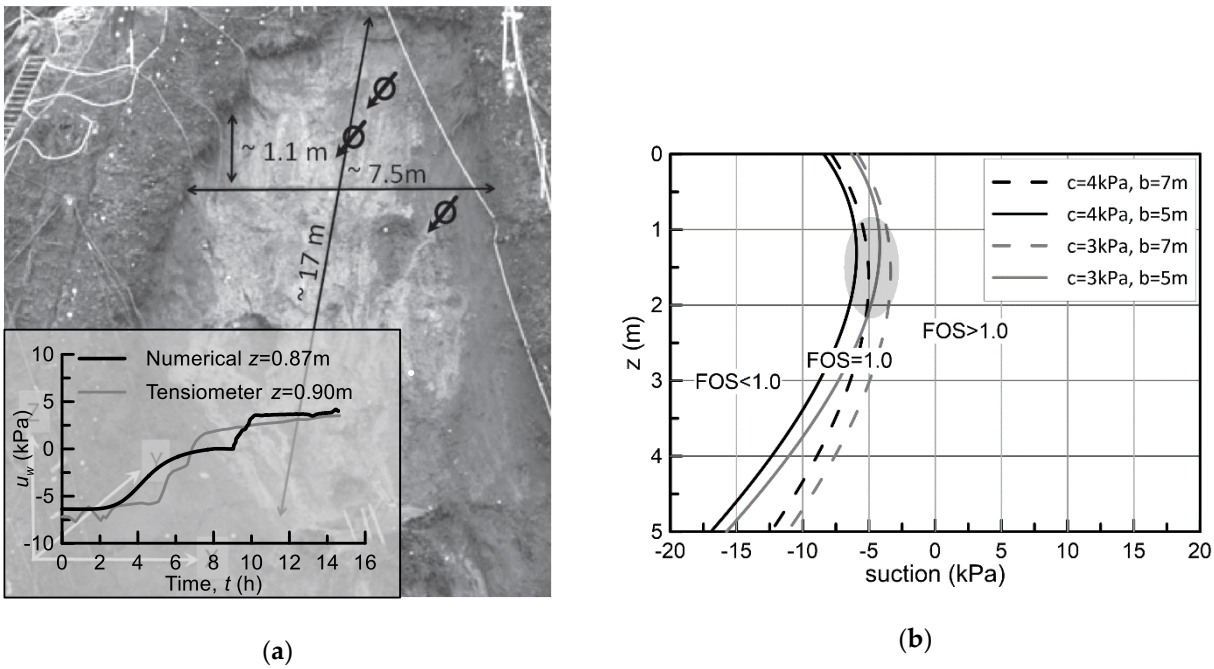

(**a**) (**b**)

Figure 10. (**a**) The Ruedlingen slope failure (after [1]) and the evolution of pore water pressure in the slope mass (after [8]); (**b**) stability curves for different combinations of cohesion and slope width which can capture well the observed instability (grey shaded area).

5. Conclusions

In this paper a limit equilibrium slope stability solution for infinite translational failure mechanisms is introduced. The solution uses Bishop's average skeleton stress to account for the increase in the shear strength under unsaturated conditions. It is extended in 3D dimensions by considering a potential limited lateral development of the failure mechanism by accounting for the lateral shear resistance that develops across the sides of the failing mass. Contrary to other similar attempts the proposed solution assumes that the lateral earth pressure coefficient (K) describes the ratio of the horizontal over the vertical Bishop's stress and not only the net stress ratio. By doing so the solution remains valid under fully saturated conditions where Bishop's average skeleton stress recalls Terzaghi effective stress.

The mechanism is evaluated using a set of actual data from a full-scale field experiment, the Ruedlingen artificial rainfall induced landslide. The proposed stability solution, despite its simplicity, can capture very satisfactory the experimentally observed behaviour. Also, its simplicity and very limited calculation cost enables an easy evaluation of different scenarios with respect to slope geometries and soil parameters which can prove very useful in back analysis of slope failures. Such simple validated tools for the analyses of engineering problems under unsaturated conditions formulated as a natural

Preprints (www.preprints.org) | NOT PEER-REVIEWED | Posted: 5 January 2021 doi:10.20944/preprints202101.0091.v1

extension of similar solution of classical soil mechanics are very important in facilitating a wider adoption of unsaturated mechanics in everyday geotechnical practice.

Appendix A

Starting from the Mohr – Coulomb criterion (Equation 7) to calculate the shear resistance as a force we multiple with the area of the failure surface which is equal to $l = 1\text{m}$ multiplied by 1m for the distance perpendicular to the examined 2D problem (analyses per running meter):

$$T = c \cdot l + \{\sigma_n \cdot l + s \cdot \chi \cdot l\} \cdot \tan\phi \quad (\text{for } l = 1\text{m}) \text{ or} \tag{A.1a}$$

$$T = c + N \cdot \tan\phi + s \cdot \chi \cdot \tan\phi \tag{A.1b}$$

In Equation A.1b, N represents the reaction force at the failure interface as this has been calculated with Equation 5 and thus, we can finally write:

$$T = c + (q + \gamma z)\ \cos^2\theta \cdot \tan\phi + s \cdot \chi \cdot \tan\phi \tag{A.2} \equiv (8)$$

Appendix B

In Equation 12 which represents the shear strength along the side of the examined mechanism, Bishop's average skeleton stress is described through Equation 11 to obtain:

$$\tau_s = c_s + \sigma_h' \cdot \tan\phi_s = c_s + \left(K \cdot q + K \cdot \gamma \cdot \frac{z}{2} + K \cdot s \cdot \chi\right) \tan\phi_s \tag{B.1}$$

Examining one side the shear strength above develops along the lateral side of the mechanism which as portrayed in Figure 1 by the light grey shaded area it is a parallelogram with area equal to $z \cdot a = z \cdot \cos\theta$. Multiplying Equation B.1 with the $z \cdot \cos\theta$, shear resistance along the side is:

$$T_s = c_s \cdot z \cdot \cos\theta + \left(K \cdot q + K \cdot \gamma \cdot \frac{z}{2} + K \cdot s \cdot \chi\right) z \cdot \cos\theta \cdot \tan\phi_s \ \text{ or} \tag{B.2a}$$

$$T_s = c_s \cdot z \cdot \cos\theta + K \cdot q \cdot z \cdot \cos\theta \cdot \tan\phi_s + K \cdot \gamma \cdot \frac{z^2}{2} \cdot \cos\theta \cdot \tan\phi_s + K \cdot s \cdot \chi \cdot z \cdot \cos\theta \cdot \tan\phi_s \tag{B.2b} \equiv (13)$$

References

1. Askarinejad, A.; Casini, F.; Bischof, P.; Beck, A.; Springman, S.M. Rainfall Induced Instabilities: A Field Experiment on a Silty Sand Slope in Northern Switzerland. *RIG (Italian Geotechnical Journal* **2012**, 50–71.
2. Tagarelli, V.; Cotecchia, F. The Effects of Slope Initialization on the Numerical Model Predictions of the Slope-Vegetation-Atmosphere Interaction. *Geosciences* **2020**, *10*, 85, doi:10.3390/geosciences10020085.
3. Cotecchia, F.; Santaloia, F.; Tagarelli, V. Towards A Geo-Hydro-Mechanical Characterization of Landslide Classes: Preliminary Results. *Applied Sciences* **2020**, *10*, 7960, doi:10.3390/app10227960.
4. Tang, A.M.; Hughes, P.N.; Dijkstra, T.A.; Askarinejad, A.; Brenčič, M.; Cui, Y.J.; Diez, J.J.; Firgi, T.; Gajewska, B.; Gentile, F.; et al. Atmosphere-Vegetation-Soil Interactions in a Climate Change Context; Impact of Changing Conditions on Engineered Transport Infrastructure Slopes in Europe. *Quarterly Journal of Engineering Geology and Hydrogeology* **2018**, *51*, 156–168, doi:10.1144/qjegh2017-103.
5. Casini, F.; Minder, P.; Springman, S.M. Shear Strength of an Unsaturated Silty Sand. *Unsaturated Soils : Proceedings of the Fifth International Conference on Unsaturated Soils, Barcelona, Spain, 6-8 September 2010* **2011**, 211–216.
6. Springman, S.M.; Jommi, C.; Teysseire, P. Instabilities on Moraine Slopes Induced by Loss of Suction: A Case History. *Géotechnique* **2003**, *53*, 3–10, doi:10.1680/geot.2003.53.1.3.
7. Zhang, L.L.; Zhang, J.; Zhang, L.M.; Tang, W.H. Stability Analysis of Rainfallinduced Slope Failure: A Review. *Proceedings of the Institution of Civil Engineers: Geotechnical Engineering* 2011, *164*, 299–316.
8. Sitarenios, P.; Casini, F.; Askarinejad, A.; Springman, S. Hydro-Mechanical Analysis of a Surficial Landslide Triggered by Artificial Rainfall: The Ruedlingen Field Experiment. *Géotechnique* **2019**, 1–14, doi:10.1680/jgeot.18.p.188.
9. Bishop, A.W.; Blight, G.E. Some Aspects of Effective Stress in Saturated and Partly Saturated Soils. *Geotechnique* **1963**, *13*, 177–197, doi:10.1680/geot.1963.13.3.177.
10. Alonso, E.E.; Pereira, J.M.; Vaunat, J.; Olivella, S. A Microstructurally Based Effective Stress for Unsaturated Soils. *Geotechnique* **2010**, *60*, 913–925, doi:10.1680/geot.8.P.002.
11. Tarantino, A. A Possible Critical State Framework for Unsaturated Compacted Soils. *Geotechnique* **2007**, *57*, 385–389, doi:10.1680/geot.2007.57.4.385.
12. Fredlund, D.G.; Xing, A.; Fredlund, M.D.; Barbour, S.L. The Relationship of the Unsaturated Soil Shear Strength to the Soil-Water Characteristic Curve. *Canadian Geotechnical Journal* **1996**, *33*, 440–448, doi:10.1139/t96-065.
13. Vanapalli, S.K.; Fredlund, D.G.; Pufahl, D.E.; Clifton, A.W. Model for the Prediction of Shear Strength with Respect to Soil Suction. *Canadian Geotechnical Journal* **1996**, *33*, 379–392, doi:10.1139/t96-060.
14. Al-Sharrad, M.A.; Gallipoli, D.; Wheeler, S.J. Experimental Investigation of Evolving Anisotropy in Unsaturated Soils. *Geotechnique* **2017**, *67*, 1033–1049, doi:10.1680/jgeot.15.P.279.
15. Askarinejad; Amin Failure Mechanisms in Unsaturated Silty Sand Slopes Triggered by Rainfall. **2015**, doi:10.3929/ethz-a-010002526.
16. Casini, F.; Jommi, C.; Springman, S. A Laboratory Investigation on an Undisturbed Silty Sand from a Slope Prone to Landsliding. *Granular matter* **2010**, *12*, 303–316, doi:10.1007/s10035-010-0182-y.
17. Brönnimann, C.; Tacher, L.; Askarinejad, A.; Kienzler, P.; Springman, S.M. Pore Water Pressure Modelling in a Rainfall Triggered Shallow Landslide. *Abstract volume : 7th Swiss Geoscience Meeting* **2009**, 280–281.
18. Springman, S.; Askarinejad, A.; Casini, F.; Friedel, S. Lesson Learnt from Field Tests in Some Potentially Unstable Slopes in Switzerland. *Acta Geotechnica Slovenica* **2012**, *1*, 5–29.
19. Askarinejad, A.; Casini, F.; Kienzler, P.; Teysseire, P.; Springman, S.M. Mountain Risks: Two Case Histories of Landslides Induced by Artificial Rainfall on Steep Slopes. In Proceedings of the Mountain risks : bringing science to society : proceedings of the "Mountain Risks" international conference, Firenze, Italy, 24-26 November 2010; CERG Editions, 2010.
20. van Genuchten, M.Th. A Closed-Form Equation for Predicting the Hydraulic Conductivity of Unsaturated Soils. *Soil Science Society of America Journal* **1980**, *44*, 892–898, doi:https://doi.org/10.2136/sssaj1980.03615995004400050002x.
21. Casini, F. Deformation Induced by Wetting: A Simple Model. *Canadian Geotechnical Journal* **2012**, *49*, 954–960, doi:10.1139/T2012-054.
22. Fraccica, A.; Romero, E.; Fourcaud, T.; Sondon, M.; Gandarillas, L. Tensile Strength of a Vegetated and Partially Saturated Soil. *E3S Web Conf.* **2020**, *195*.